INVITED REVIEW PAPER

A review on the recent developments of ruthenium and nickel catalysts for CO_x-free H_2 generation by ammonia decomposition

Thien An Le[‡], Quoc Cuong Do[‡], Youngmin Kim, Tae-Wan Kim, and Ho-Jeong Chae[†]

Chemical & Process Technology Division, Korea Research Institute of Chemical Technology,
141 Gajeong-ro, Yuseong-gu, Daejeon 34114, Korea

Abstract−The emerging H_2 economy faces storage and transport challenges, and the use of ammonia (NH_3) as a CO_x-free source of H_2 via NH_3 decomposition has recently attracted attention. Noble Ru-based catalysts are considered the best choice for highly efficient NH_3 decomposition; however, their high cost and limited availability are disadvantages in large-scale applications. Otherwise, among non-noble metal-based catalysts, Ni-based catalysts are the most active, and Ni is considered a good alternative candidate material for NH_3 decomposition because of its low cost. At present, some challenges remain in efforts to improve the efficiency of both Ru- and Ni-based systems. This review covers recent developments regarding these catalysts and can serve as a comprehensive work for evaluating effective long-term strategies.

Keywords: Ni-based, Ru-based, Kinetics, Mechanism, Support, Promoter, Ammonia (NH_3) Decomposition, Hydrogen Production/Generation

INTRODUCTION

The development and commercialization of energy technologies is imperative for a clean and sustainable energy future and environmental sustainability. Reducing CO_2 emissions associated with fossil fuel utilization has fostered an interest in sustainable energy development. Hydrogen (H_2) energy is considered a viable future replacement for fossil-fuel, with fewer potential effects on the climate [1,2]. H_2 can help reduce or eliminate regulated greenhouse gas emissions currently produced by the N_2O hydrogenation [3]
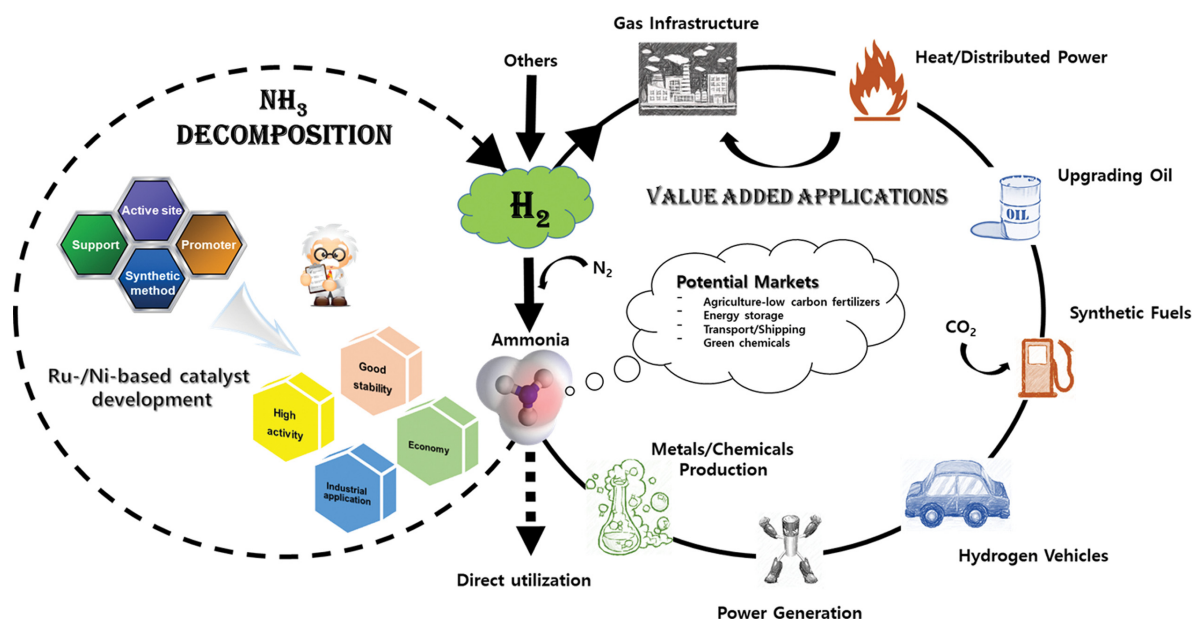

Fig. 1. H_2 production based on a catalyzed NH_3 decomposition study merging the value H_2 usage-pathways.

[†]To whom correspondence should be addressed.
E-mail: hjchae@krict.re.kr
[‡]These authors contributed equally to this work.

and methanation processes [4]. Presently, high purity on-site H_2 feedstocks are required for proton exchange membrane fuel cells (PEMFCs) to avoid poisoning the electrode and not decrease cell efficiency [5,6]. H_2 has a low volumetric energy density in compressed gas and liquid forms, so there are still significant challenges associated with H_2 delivery and storage. Various chemicals and stable states have recently been investigated for potential H_2 storage and production capacity [7]. Ammonia (NH_3) is a promising hydrogen carrier because of its high H_2 content (17.8% by weight and 121 kg_{H_2}/m^3 by volumetric density at 10 bar). NH_3 has recently been recognized as one of the perfect molecules combined with H_2 [8,9], which shows advantages for H_2 production via NH_3 decomposition process. This technology can meet the near-zero carbon H_2 generation requirement, giving it a very low carbon footprint. The approach is now being studied and applied in both academic and industrial sectors [5,6,9-11]. Fig. 1 shows H_2 production based on a catalytic NH_3 decomposition study, merging the value H_2-usage pathways.

Numerous innovative catalysts have been developed for low-temperature NH_3 decomposition, especially at a high space velocity (SV) [11-13], in which ruthenium (Ru) has been the most active metal among the catalytic systems studied so far. Although Ru-based catalysts present good performance in NH_3 decomposition, the scarcity and high cost of this precious metal are the main limitations for large-scale applications. Alternatively, nickel (Ni) has been reported as the best performing catalyst among the non-noble metal catalysts for NH_3 decomposition [14,15] with a cost advantage, which can be a promising alternative catalyst in this field. During the past two decades, Ru- and Ni-based catalysts have been predominantly studied for NH_3 decomposition (Fig. 2). Their recent development has focused on high catalytic performance at low temperature for CO_x-free H_2 production and relied on several approaches, including the selection and modification of supports, the addition of promoter elements, the formation of multi-active sites catalysts, and the innovation of catalyst fabrication methods.

Therefore, it is of great significance to summarize the recent research progress in developing Ru- and Ni-based catalysts applied in this field. This review will introduce the fundamental concepts of NH_3 decomposition, including a summary of the reaction mechanism and kinetics of the reaction over Ni- and Ru-based catalysts. Next, based on the recent developments regarding both catalysts, the outstanding developed strategies to enhance their catalytic performance will be thoroughly discussed.
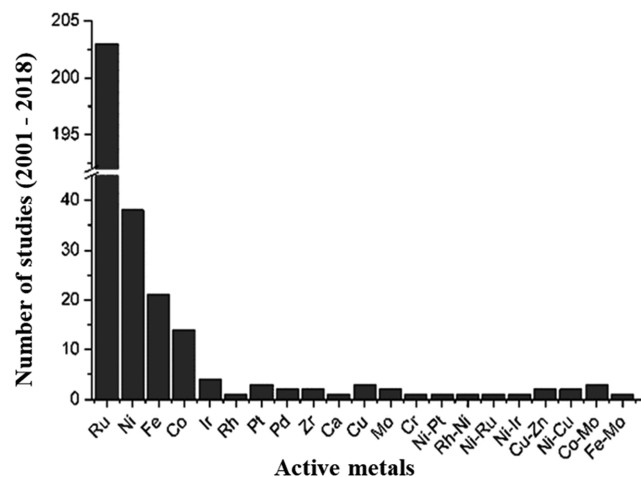
KINETICS AND MECHANISMS OF Ru- AND Ni-BASED CATALYSTS

Over metals, NH_3 decomposition is known as the endothermic reaction (Eq. (1)), proceeding through a stepwise dehydrogenation of adsorbed NH_3 on the active metal surface followed by recombination of two N (ad) and two H (ad) atoms to form N_2 and H_2, followed by desorption.

$$2NH_{3(g)} \leftrightarrows N_{2(g)} + 3H_{2(g)} \qquad \Delta H^0 = 46.22 \text{ kJ/mol} \qquad (1)$$

$$NH_3 \text{ (g)} \rightarrow NH_3 \text{ (ad)} \qquad (R1)$$

$$NH_3 \text{ (ad)} \rightarrow NH_2 \text{ (ad)} + H \text{ (ad)} \qquad (R2)$$

$$NH_2 \text{ (ad)} \rightarrow NH \text{ (ad)} + H \text{ (ad)} \qquad (R3)$$

$$NH \text{ (ad)} \rightarrow N \text{ (ad)} + H \text{ (ad)} \qquad (R4)$$

$$2N \text{ (ad)} \rightarrow N_2 \text{ (ad)} \qquad (R5)$$

$$2H \text{ (ad)} \rightarrow H_2 \text{ (ad)} \qquad (R6)$$

$$N_2 \text{ (ad)} \rightarrow N_2 \text{ (g)} \qquad (R7)$$

$$H_2 \text{ (ad)} \rightarrow H_2 \text{ (g)} \qquad (R8)$$
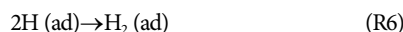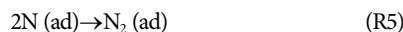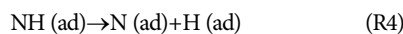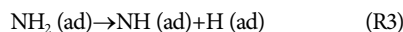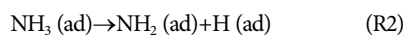
The NH_3 decomposition reaction rate (r_{NH_3}) is described by the power-law model as follows:

$$r_{NH_3} = k' P_{NH_3}^{\alpha} P_{H_2}^{\beta} \qquad (2)$$

where P_{NH_3}, P_{H_2}, α, and β are the partial pressures of NH_3, and H_2, and the reaction order of NH_3, and H_2, respectively. The H_2 order values for both Ru- and Ni-based catalysts are negative, indicating that H_2 inhibited the NH_3 decomposition reaction. In general, H_2 is like an inhibitor on the NH_3 decomposition rate while H_2 is co-fed along with NH_3, particularly at low temperature and a high H_2 partial pressure [16-18]. The power-law model here could investigate the effects of the different operation variables on the reactions; however, it is inconvenient to detail the Ru or Ni size effects because both α and β always vary simultaneously.

The other concept, the Temkin-Pyzhev kinetic, supposes N (ad) associative desorption as the rate-determining step in NH_3 decomposition [18-20], and the corresponding rate equation is generally described as follows:

$$r_{NH_3} = k_0 \exp\left(-\frac{E_{app}}{RT}\right) P_{NH_3}^{\alpha} P_{H_2}^{\beta} \qquad (3)$$

where k_0 and E_{app} are the pre-exponential factor and the activation energy, respectively. Some studies have investigated the steady-state decomposition kinetics of NH_3 using a single-crystal approach [16, 19-21]. The results were compared with those of some specific catalysts, as shown in Table 1, indicating the steps occurring on active

Fig. 2. Compilation of active metals studied in the NH_3 decomposition literature from 2001 to 2018 (reproduced with permission from ref. [119], copyright 2020, Royal Society of Chemistry).

Table 1. Kinetic parameters were reported for NH₃ decomposition over Ru-based catalysts. Data sourced from ref. [16]

Catalyst	T (K)	P_{NH_3} (Torr)	$r_{NH_3} = k_0 \exp\left(-\dfrac{E_{app}}{RT}\right) P_{NH_3}^{\alpha} P_{H_2}^{\beta}$		
			E_{app} (kcal/mol)	α	β
Ru(001)	<650	2×10^{-6}	43±3	0	-
	>750	2×10^{-6}	5±3	1	-
Ru(1110) & Ru(001)	<500	1×10^{-8} to 1×10^{-5}	-	0	-
	520	1×10^{-7}	-	0.4	−0.6
	>600	1×10^{-8} to 1×10^{-5}	-	1	0
Ru/Al₂O₃	673-1,073	152 to 760	33	0 to 1	-
Ru film	543-738	10 to 53	45	1.2	−2
Ru/Al₂O₃	623-673	600 to 800	31	0.6	−0.9
Ru	825-1,009	-	59	1.0	−1.75
Ru/Al₂O₃	623-723	10 to 90	21	-	-
Ru/C	623-723	10 to 90	23±1	0.69 to 0.75	−2 to −1.6

sites, not on low-indexed flat terraces. The results also suggest that morphologically "rough" particles could lead to more abundant steps than the equilibrated flat forms of the bulk or well-structured particles.

Many mechanisms have been proposed based on measurements at conditions far from those relevant for NH₃ decomposition to generate pure H₂. Nevertheless, irrespective of the specific catalysts, there are two possible rate-limiting steps: (1) cleavage of the first N-H bond resulting in the formation of NH₂ (ad) and H (ad), or (2) the recombination of N (ad) resulting in the desorption of N₂. The binding energy of the N (ad) atom on the active metal surface is a good descriptor for NH₃ decomposition [22-24]. This binding energy must be strong enough for dehydrogenation of the NH$_x$ species to occur but sufficiently weak so that the recombinative N₂ desorbs from the surface to complete the catalytic cycle. As an


Fig. 3. A correlation between the NH₃ decomposition rate on several metals and the relative rate of the N-H bond scission and N-N recombination as estimated from the Blowers-Masel correlation (reproduced with permission from ref. [25], copyright 2004, Springer Nature).

essential reference for comparing different active metals, Fig. 3 shows the correlation between the NH₃ decomposition rate on several metals and the relative rate of the N-H bond scission and N-N recombination as estimated from the Blowers-Masel correlation [25]. The rate-controlling step is considered as either breaking the first N-H bond of the NH₃ molecule (Eq. (R2)) or the recombinative desorption of N (ad) atoms (Eq. (R7)). The breaking of the first N-H bond of the NH₃ molecule requires the highest energy than the remains, so if the dissociation energy of the first N-H bond of the NH₃ molecule is higher than the energy of the N (ad) atoms recombinative desorption, the cleavage of the first N-H bond of the NH₃ molecule (Eq. (R2)) is the rate-controlling step, in contrast, the recombinative desorption of the N (ad) atom (Eq. (R7)) is the rate-controlling step. Takahashi and Fujitani et al. [18] studied NH₃ decomposition over Ni/MgO and Ru/MgO and found the difference from the mechanism; the recombinative N₂ desorption is the rate-limiting step on the Ru-based catalyst, whereas the overall rate of NH₃ decomposition is controlled by the dehydrogenation of the NH$_x$ species on the Ni-based catalyst. Therefore, it is worth exploring reducing the barrier to NH₃ dehydrogenation on the Ni surface to improve the catalytic performance further. Ganley et al. [25] also concluded that the concept is rate-limiting for Ni-based catalysts, while for Ru, the N-H bond scission is limiting based on computational investigations. It appears that there is probably no general and straightforward answer for which is the rate-determining step in the NH₃ decomposition, N-H cleavage, or the N₂ desorption. So, each system needs to be analyzed in detail by a specific reaction condition.

Concerning the size effect on the mechanism, Zheng et al. developed very detailed kinetic models for Ru/Al₂O₃ by [26]. In this study, the optimum Ru size (2.2 nm) in the range of 1.9-4.6 nm shows the highest activity towards the NH₃ decomposition. The recombinative desorption of the surface N atom that acts as the rate-determining step here is claimed by the well-fitting between experimental data and the Temkin-Pyzhev model. In Fig. 4(a), the NH₃ decomposition is highly structurally sensitive, with turnover frequency (TOF) values increasing by almost two orders of magnitude as the Ru particle size increases from 0.8 to >7 nm [27]. In
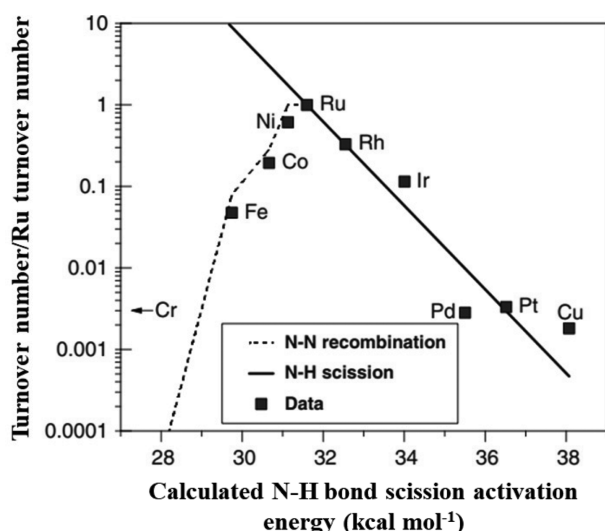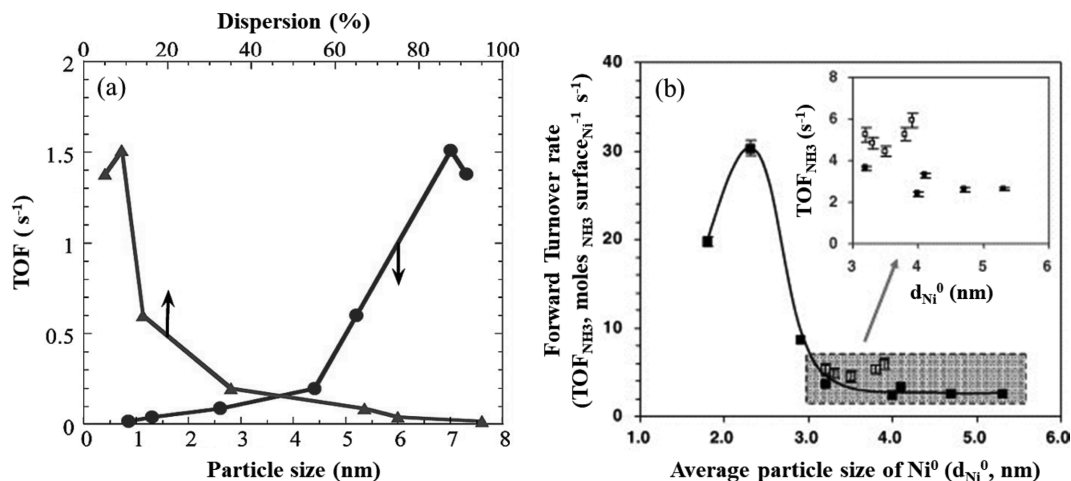
Fig. 4. (a) TOF for NH₃ decomposition as a function of Ru particle size (circles) and Ru dispersion (triangles) over 4 wt% Ru/Al₂O₃ (reproduced with permission from ref. [27], copyright 2009, American Chemical Society), (b) The forward NH₃ turnover rate for NH₃ decomposition as a function of Ni⁰ particle size (solids: Ni/Al₂O₃; hollows: Ni/La-Al₂O₃) (reproduced with permission from ref. [17], copyright 2005, Elsevier BV).

that report, the results of the experiments and first-principle simulations indicated the calcination pretreatment is the critical step to control the particle shape and gives rise to the flat Ru nanoparticles, which maximizes the number of active (B_5) sites. These so-called B_5 sites employed by the density functional theory (DFT) calculations have adsorption energy, facilitating the desorption of N_2 molecules [28]. The maximum TOF and number of active (B_5) sites were obtained at ~7 nm for elongated nanoparticles and ~1.8-3 nm for hemispherical nanoparticles. Consequently, the particle shape determination is very important to develop quantitative particle size/shape-activity relations. NH_3 conversion rate decline with the increase of Ni crystallite size in Ni/Al₂O₃ has been verified by Zhang et al. [17], as shown in Fig. 4(b), with the high TOF obtained with a Ni crystallite size range from 1.8-2.9 nm. The rate-determining step here is determined by the recombinative desorption of N_2 following the Temkin-Pyzhev mechanism. Duan et al. [29] proposed that the optimum Ni particle size around 3.1-3.6 nm in Ni/MCM-41 catalysts can decrease the energy barrier of the N_2 associative desorption. Chen et al. [30] studied the size effects of the octahedral Ni towards the NH_3 decomposition reaction with four different Ni nanoclusters (Ni_{19}, Ni_{44}, Ni_{85}, and Ni_{146}) via DFT calculations. The results revealed that these four Ni nanoclusters adopted the same NH_3 decomposition mechanism, in which the N_2 desorption process is the rate-determining step and the predicted catalytic activity decreases in the order of $Ni_{44} > Ni_{146} \approx Ni_{85} > Ni_{19}$. Moreover, molecular dynamics calculations suggested that the nanoclusters with larger size show better thermal stability due to their high cohesive energy and low changes of interatomic distances in the Ni-Ni bond length.

RECENT DEVELOPMENTS OF Ru- AND Ni-BASED CATALYSTS FOR NH₃ DECOMPOSITION

1. Ru-based Catalysts

The Ru-based materials are reported as the most effective cata-

lysts for low-temperature NH_3 decomposition based on their electronic promotion possessing an optimum N_2 binding energy; the surfaces for the desired catalytic activity have been identified by the heat of N_2 chemisorption [24].

1-1. Support

The NH_3 decomposition activity of Ru-based catalysts is often higher than that of the others; however, it varies much depending on the exact nature of the catalyst. The support can influence the catalytic property by regulating the size distribution, morphology, electronic state of the active metal. The catalytic performance of Ru supported on different support materials was studied and published; most of the studies have shown that the use of high-basic supports like MgO [31-33], or neutral supports such as carbon nanotubes (CNTs) [34,35], results in better catalytic properties compared to the amphoteric supports Cr_2O_3 [36] and, TiO_2 [5], or high-acidic supports like Al_2O_3 [5,11,33,37-39], ZrO_2 [40,41], SiO_2 [42, 43]. Recently, rare earth metal oxides, CeO_2 [38,44-46], La_2O_3 [47, 48], and Pr_6O_{11} [49,50], have attracted many researchers due to their structural and electronic properties in catalysis applications for NH_3 decomposition. Fig. 5(a) shows the highest NH_3 decomposition activity of a supported-Ru on La_2O_3 compared to Er_2O_3, Al_2O_3, SiO_2, and TiO_2; the basicity of the support has been confirmed as an important role in the catalytic activity of supported-Ru samples [47]. The comparative data of supported-Ru samples were collected and shown in Table 2.

So far, CNTs have proven to be the most suitable support for Ru in NH_3 decomposition, mainly due to their electronic conductivity [5,34]. Nevertheless, the high-cost limitation of commercial CNTs interferes with using Ru/CNTs catalysts on an industrial scale. The modification of carbon materials by nitrogen doping enhanced low-temperature NH_3 decomposition of Ru nanoparticles, with a production yield higher than the corresponding value for unmodified CNTs supports, despite having similar Ru particle sizes [12]. That work simultaneously increased the conductivity and basicity of the support, electronically modifying the Ru active sites, and
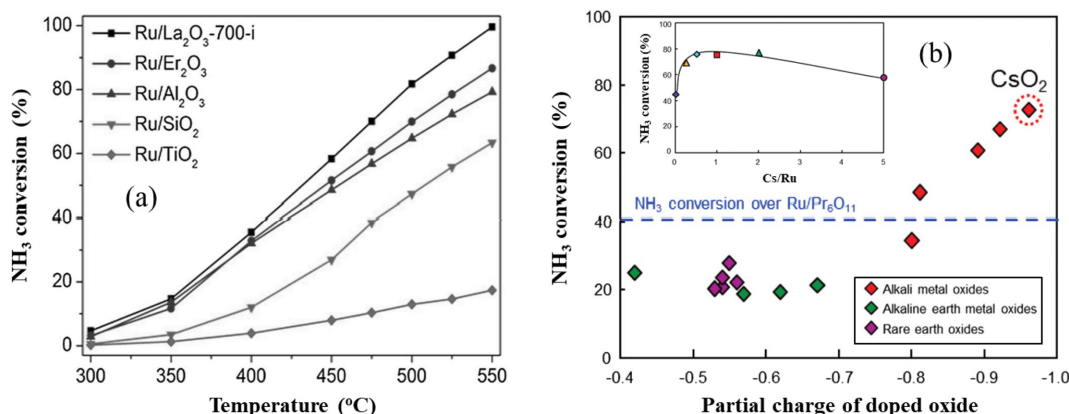
Fig. 5. (a) NH$_3$ conversion for NH$_3$ decomposition over Ru catalysts supported various metal oxides (reproduced with permission from ref. [47], copyright 2019, Elsevier BV), (b) NH$_3$ conversion at 350 °C for 5 wt% Ru/Pr$_6$O$_{11}$ doped with various oxides (dopant/Ru ratio=1) vs. partial charge of doped oxide (reproduced with permission from ref. [50], copyright 2014, Elsevier BV).

promoted a strong metal-support interaction (SMSI). The porous and graphitic structures of the carbon support significantly affected the catalytic NH$_3$ decomposition [51]; the 3-4 nm-size Ru particles with the assistance of graphitic carbons improved the catalytic performance, while the surface area of the carbons was less important.

As an allotrope of carbon, graphene can also support Ru for the NH$_3$ decomposition process [52]. Graphene seems to be considered much more advantageous than CNTs for high Ru dispersion as well as high Ru loading capacity. The improvement of metal dispersion, the optimum size, and the suitable morphology of the Ru nanoparticles on graphene resulted in a highly enhanced catalytic performance for NH$_3$ decomposition. However, the catalytic activity of Ru/graphene is not stable and decreases gradually at 500 °C, which is mainly due to the methanation of the graphene nanosheet and the sintering phenomenon under high temperatures. Carbon nanofibers (CNFs), a fish-bone graphene alignment and CNTs, are better than CNTs on identically sized Ru crystals due to their active oxygen groups [53]. In general, using carbon sources as the support always includes a side methanation reaction, which is adverse for catalyst stability while operating at a relatively high temperature. Thus, using a non-carbon support material in the catalyst design is preferred to avoid these potential issues. It has recently led to the rapid development of multi-metallic oxides; they exhibit properties that do not merely originate from the individual monometallic oxide [13,39,41,54-57]. Recent works have shown that the incorporation of La into MgO [35,48,58,59], ZrO$_2$ [40,41], and Al$_2$O$_3$ [13,60] enhances their NH$_3$ decomposition activity at a low temperature. Barium hexaaluminate (BHA) supports Ru for a higher catalytic performance than Ru/CNTs [39]. Mg-Al mixed oxide is derived with a precursor of Mg$_2$Al-layered double hydroxide (Mg$_2$Al-LDH) used to load the Ru to develop the Ru/Mg$_2$Al-LDO catalyst for hydrogen production through NH$_3$ decomposition [33]. A strong SMSI over Ru/CaAlO$_x$ produced by the surface structural reconstruction of Ca-Al LDH to Ca-Al LDO (hydroxide-to-oxide transformation) improves the catalytic NH$_3$ decomposition at low-temperature zone [54]. Our group has developed La$_x$Ce$_{1-x}$O$_y$ materials as potential supports for Ru with a reported

highly efficient NH$_3$ decomposition [61]. The Ru/La$_{0.33}$Ce$_{0.67}$ catalyst showed outstanding performance at a low temperature (below 450 °C) and maintained its outperformance for more than 100 h under critical reaction conditions (54,000 mL$_{NH3}$/g$_{cat.}$/h of GHSV).

An inorganic electride, [Ca$_{24}$Al$_{28}$O$_{64}$]$^{4+}$(e$^-$)$_4$, abbreviated C$_{12}$A$_7$:e$^-$, was developed and achieved a low E$_{app}$ (64 kJ mol^{-1}) of recombinative N$_2$ desorption. Ru/ C$_{12}$A$_7$:e$^-$ is highly active (TOF~12 s^{-1} at 400 °C) and durable for NH$_3$ decomposition, due to the low work function of the chemically stable C$_{12}$A$_7$:e$^-$. The electron injection from C$_{12}$A$_7$:e$^-$ to Ru accelerates Ru-N bond dissociation [62]. Nanometer- and sub-nanometer-sized Ru particles with approximately 1.0 nm were deposited successfully on some alkali-exchanged zeolite Y supports and showed good catalytic performance in the order of Ru/Rb-Y>Ru/K-Y>Ru/Na-Y>Ru/H-Y [63]. Here, the open-pore structure and high basicity of the Rb-Y zeolite led to high Ru dispersion with strong SMSI for high catalytic activity. The improved catalytic performance was consistent with the decrease in support acidity, which was correlated with the increase in electron enriched-Ru species. A natural halloysite nanotubes (HNTs) clay has been used to support Ru nanoparticles [64]. Although its catalytic performance is not comparable to Ru/CNTs, the HNTs still have advantages, such as low price and abundance, and can be further advanced by improving the synthesis procedure.

Some amide materials have been reported to show considerable NH$_3$ decomposition activity [65]. So, many researchers combined these materials with Ru to decompose NH$_3$; Ba(NH$_2$)$_2$ and Ca(NH$_2$)$_2$ are neither electronic nor structural materials but can be used to support Ru for high-performance NH$_3$ decomposition at low-temperature [44]. In a NH$_x$-rich environment, Ru mediates the electron transfer from NH$_x$ to facilitate NH$_x$ coupling, to release N$_2$ and H$_2$ easily. A higher TOF and lower E$_{app}$ were observed over Ru-Ba(NH$_2$)$_2$ and Ru-Ca(NH$_2$)$_2$ catalysts, compared to Ru-Mg(NH$_2$)$_2$ and Ru/MgO catalysts. This indicates the different roles of Ba(NH$_2$)$_2$/Ca(NH$_2$)$_2$ and Mg(NH$_2$)$_2$/MgO in the NH$_3$ decomposition process. In this study, the catalysis mechanism over Ru-Ca(NH$_2$)$_2$ and Ru-Ba(NH$_2$)$_2$ was described to follow two main steps: (1) the decomposition of amides to H$_2$, N$_2$, and imides by Ru and (2) the regeneration of amides by the reaction of imides

Table 2. Catalytic activity of the supported Ru catalysts for NH₃ decomposition

Catalyst	Ru content (wt%)	$T_{reaction}$ (°C)	GHSV ($mL_{NH_3}/g_{cat.}/h$)	X_{NH_3} (%)	r_{H_2} (mmol/min/$g_{cat.}$)	TOF_{H_2} (s^{-1})	Ref.
Ru/fumed-SiO₂	5.0	450	30,000	49.7	16.7	-	[42]
Ru/SBA-15				49.0	16.4	-	
Ru/c-MgO	2.9	450	30,000	75.0	25.1	3.9	[31]
Ru/CNTs	5.0	450	30,000	43.7	14.6	-	[72]
Ru/AC				28.7	9.6	-	
Ru/ZrO₂				24.8	8.3	-	
Ru/MgO	4.6	450	30,000	33.7	11.3	0.6	[33]
Ru/Mg₂Al-LDO	4.6			42.7	14.3	1.5	
Ru/Al₂O₃	4.6			34.8	11.7	0.9	
Ru/Cr₂O₃	5.0	450	30,000	10.0	3.3	0.3	[36]
Ru/TiO₂-w	4.8	450	30,000	5.3	1.7	1.3	[34]
Ru/CNTs	4.8	450	60,000	18.8	12.9	-	
Ru/Ba-ZrO₂	3.0	450	30,000	23.6	7.9	5.2	[41]
Ru@La-ZrO₂ (LSZ)	3.0	450	30,000	80.0	27.3	-	[40]
Ru/La₂O₃-700-i	4.8	450	18,000	58.2	11.7	2.4	[47]
Ru/Er₂O₃				51.8	10.4	-	
Ru/La(20)-Al₂O₃	1.1	450	5,000	81.0	4.5	0.7	[120]
Ru/CNTs	2.5	450	30,000	17.0	5.8	1.1	[39]
Ru/BHA	2.7			40.0	13.8	2.9	
Ru/CeO₂	2.0	400	13,800	77.0	11.9	1.8	[38]
Ru/CeO₂ (NR)	1.0	450	22,000	98.0	24.0	-	[45]
Ru/Pr₆O₁₁	5.0	450	3,000	100	3.3	0.3	[50]
Ru/La₂O₃	1.0	450	3,000	96.5	3.2	-	[49]
Ru/Pr₆O₁₁				95.4	3.2	-	
Ru/MgO				84.2	2.8	-	
Ru/N-CNT₁	7.0	400	6,000	48.0	3.2	4.3	[12]
Ru/CNTs				33.9	2.3	3.1	
Ru/MWCNTs	2.03	450	6,000	85.4	5.7	2.0	[77]
Ru/graphitic C	5.0	550	30,000	95.0	29.1	2.6	[51]
Ru/C#	0.91	600	20,000	78.2	17.4	2.7	[76]
CS60 Ru/graphene	42.0	450	20,000	90.1	20.1	-	[121]
Ru/CNFs	3.2	450	6,500	77.5	5.6	0.3	[53]
Ru/CaAlOₓ-w	2.5	450	6,000	72.0	4.8	-	[54]
Ru/La₀.₃₃Ce₀.₆₇	1.8	450	6,000	100	6.7	2.7	[61]
			30,000	79.3	26.5	11.4	
Ru/C₁₂A₇: e⁻	2.2	400	15,000	70.0	11.7	11.5	[62]
Ru/Rb-Y	1.96	450	30,000	23.0	7.7	0.8	[63]
Ru/H-Y	2.10			16.0	5.4	0.6	
Ru/HNTs	2.6	450	12,600	24.0	3.4	2.6	[64]
Ru/Ba(NH₂)₂	4.4	400	60,000	18.0	8.1	1.3	[44]
Ru/Ca(NH₂)₂	4.6			7.0	4.6	0.4	
Ru/MPC-ZrO₂	2.0	450	6,000	15.0	1.0	0.1	[66]

with NH$_3$. Another study recently demonstrated the potential use of metal-organic frameworks (MOFs) as templates for Ru-supported catalysts. Ultra-small Ru (<3 nm) was stably impregnated on UiO-66(Zr)-NH$_2$ and presented a TOF considerably higher than that of Ru/CNTs for NH$_3$ decomposition at low temperature [66]. Unfortunately, the Ru accessibility was limited because the MOF framework structures could be easily collapsed by high-temperature calcination.

1-2. Promoted Catalysts, Multi-active Sites Catalysts, and Alloy Catalysts

To facilitate the recombinative N$_2$ desorption step in Eq. (R7), promoters are added as an electron donor agent. A recent study on the temporal analysis of products (TAP) revealed substantial differences for activated carbon (AC)-supported Ru catalyst with and without a Na promoter [67]. That study reported a Na-N-Ru complex formation within the Ru crystallites and suggested that Na prevents hydrogen diffusion from the metal to the support via spillover. The reaction apparent E$_{app}$ could be decreased due to the modification of the electronic Ru state by introducing the alkalis group (electronic promoters) [68]. Mg and Ca belong to the alkaline group studied as the structural promoters, whereas Ba could play two roles in electronic and structural promotion [69,70]. Although the modification of CNTs with nitrogen could enhance the catalytic activity of Ru/N-CNTs [12], the performance of Ru supported by a K-doped CNTs system was found to be better than that of the Ru/N-CNTs [34]. Those studies confirmed that easy electron transfer and high Ru dispersion are the main factors contributing to the good NH$_3$ decomposition activity of the Ru/CNTs. The performance ranking of K>Na>Li>Ce>Ba>La>Ca in Ru/CNTs was reported by Yin et al. [5], while the order K>Na>Ca>Li was reported for Ru/CMK-3 by Zhu et al. [71]. The order K>Na>Li>Ba>Ca, with Ce and La at intermediate levels of promoting activity, was reported for Ru/CNTs by Wang et al. [34]. Notably, the promotion was also sensitive to the type of support. For example, K-Ru/CNTs showed better catalytic performance than K-Ru/MgO for NH$_3$ decomposition [72]. Cs modification improved the catalytic activity tenfold more than Ba modification over Ru/MgAl$_2$O$_4$ [73]. In Fig. 5(b), Cs$_2$O was confirmed as the most effective dopant compared to the alkali, alkaline, or rare-earth metal oxides promoting Ru/Pr$_6$O$_{11}$. The best Cs/Ru ratio, 0.5-2, effectively promotes without adverse effects from the coverage by Cs$_2$O on the Ru surface [50]. Recently, Cs$_2$O has been used to promote Ru/CeO$_2$, exhibiting a high catalytic activity [46]. In general, the promoter addition to the Ru-based system increases the basicity of the materials, which is claimed as a beneficial property for H$_2$ production from NH$_3$. For instance, the basicity enhancement of base-treated ZrO$_2$ by La, K, and Ba was suggested to have the strongest influence in doping Ru particles, which were found to be highly effective catalysts for NH$_3$ decomposition [40,41,74,75]. As a result, the addition of small amounts of promoters, such as alkali, alkaline earth metal, or rare earth metal oxides and hydroxides, help enhance the Ru-based catalytic activity. However, the promotional capability and promoting mechanism of these promoters are still controversial. The comparative data regarding promoted catalysts are presented in Table 3.

The promising trends for NH$_3$ decomposition include multi-

active sites and alloy catalysts. Yang et al. [52] recently prepared Ru and Ru-Co clusters supported by zeolitic imidazolate frameworks (ZIFs) exhibiting excellent catalytic activity and demonstrating a practical design that decomposed NH$_3$ efficiently. Li et al. [76] found that a porous graphite carbon-supported Ru-Fe cluster was better than a mono-Ru metal-supported one for NH$_3$ decomposition. The same result was also achieved when prepared bimetallic catalysts consisting of Ru and Fe were prepared on multi-walled carbon nanotubes (MWCNTs). A high specific rate (16.2 mol$_{NH3}$/g$_{Ru}$/h) with excellent stability was obtained [77]. The catalytic improvement was explained from a lower N (ad) coverage on the Ru-Fe alloy surface, which promoted the fast N (ad) desorption. A DFT investigation of core-shell Ru@Ni for the NH$_3$ decomposition reaction shows the catalytic performance comparable to that of a single metal Ru [78]. Moreover, a series of bulk Ru-based intermetallic compounds (Ru$_m$M$_n$, M=Ce, Dy, Ge, La, Nb, Sc, Si, Ta, Ti, Y, Zr) are being studied [79] ; Ru$_2$La is found to be more active than the others. Based on this result, a Raney-type Ru-La catalyst was prepared by base treatment of the ternary intermetallic compound Ru$_2$LaAl$_{10}$, which performs a high catalytic NH$_3$ decomposition activity.

1-3. Synthetic Methods

The high activity of the Ru-based catalysts is strongly related to the Ru particle size (~3-5 nm), where the B$_5$ active site amount is maximized and to the synergetic effect of supports and promoters [11,35]. Moreover, SMSI, consisting of the formation of an oxide layer covering the surface of the supported metal particles, has been reported to be key in reducibility control and an important bridge for electron transfer between metal and support, improving activity and stability [41,80]. Regarding the control of active sites and SMSI aspects, this section updates the fabrication processes for Ru-based catalysts used for NH$_3$ decomposition. Table 4 shows more detailed comparative data of some specific Ru-based catalysts synthesized under different procedures.

Wetness impregnation (WI), a conventional process for preparing Ru-based catalysts for NH$_3$ decomposition, usually produces relatively large clusters with a broad size distribution. A small amount of particles with active-structured sites (B5) contributes to the overall activity, which allows a smaller amount of the precious metal to be used. Thus, Ru-based catalysts synthesized under the WI process often have a lower catalytic activity than those synthesized by other catalyst fabrication processes [32,81]. Moreover, the Ru trichloride (RuCl$_3$·xH$_2$O) precursor is popularly used to prepare Ru-based catalysts; the difficulty in removing the residual chlorine ions (Cl$^-$), a potent inhibitor [13], in the synthetic process has a negative effect on catalytic performance. Thus, some other Ru precursors such as Ru nitrosyl nitrate, Ru acetylacetonate could be used [27,82]. Ru doped on a ZrO$_2$, CeO$_2$ support was prepared by WI, and the subsequent reduction by NaBH$_4$ or washing with aqueous NH$_3$ for free Cl$^-$ showed improvement of the catalytic NH$_3$ decomposition [46,83]. Except for the mentioned drawbacks, the WI method is still widely applied as a facile method to investigate the effects of supports or promoters generally [84].

Ru/MgO synthesized by the deposition-precipitation (DP) method (Ru/MgO-DP), which generates high Ru dispersion, high surface area, and plenty of mesopores, showed higher activity and better

Table 3. Catalytic activity of the promoted Ru-based catalysts, the multi-active sites catalysts, and alloy catalysts included Ru for NH_3 decomposition

Catalyst	Ru content (wt%)	Promoter/Ru (atomic ratio)	$T_{reaction}$ (°C)	GHSV ($mL_{NH_3}/g_{cat.}/h$)	X_{NH_3} (%)	r_{H_2} (mmol/min/$g_{cat.}$)	TOF_{H_2} (s^{-1})	E_{app} (kJ/mol)	Ref.
Li-Ru/CNTs					50.4	34.3	-	63.8	
Na-Ru/CNTs					64.8	44.0	-	60.8	
K-Ru/CNTs					84.8	57.5	-	54.2	
Ca-Ru/CNTs	4.8	1.0	450	60,000	24.1	16.1	-	70.2	[34]
Ba-Ru/CNTs					30.1	20.5	-	65.2	
La-Ru/CNTs					27.8	18.8	-	66.7	
Ce-Ru/CNTs					41.0	27.4	-	62.7	
K-Ru/Ba-ZrO_2	3.0	0.5	450	30,000	32.5	10.9	-	70.7	[75]
Cs-Ru/Ba-ZrO_2					37.8	12.7	-	64.2	
K-Ru/MgO-DP	3.5	1.0	450	36,000	64.0	25.7	-	65.9	[32]
		0.5			87.0	35.0	-	57.8	
Cs-Ru/MgO	2.8	2.0	500	60,000	88.2	59.1	-	-	[81]
K-Ru/MgO					84.0	56.3	-	-	
Ru-K/CaO	5.0	2.0*	450	9,000	91.0	9.1	3.6	75.0	[68]
Cs-Ru/C	9.1	1.5	400	57,000	27.0	17.2	1.5	134.0	[70]
Ba-Ru/C		0.43			12.0	7.5	0.6	158.0	
Ru/CMK-3					22.7	7.0	-	-	
Ru-Li/CMK-3					15.2	4.7	0.3	-	
Ru-Na/CMK-3	5.0	-	550	30,000	50.8	15.6	-	-	[71]
Ru-K/CMK-3					78.9	24.2	1.6	-	
Ru-Ca/CMK-3					48.5	14.9	-	-	
K-Ru/CNTs	5.0	1.0	450	30,000	97.3	32.6	-	-	[72]
Ru-Cs/Pr_6O_{11}					100	3.3	-	-	
Ru-Rb/Pr_6O_{11}					97.7	3.3	-	-	
Ru-K/Pr_6O_{11}					95.7	3.2	-	-	
Ru-Na/Pr_6O_{11}					87.1	2.9	-	-	
Ru-Mg/Pr_6O_{11}	5.0	1.0	400	3,000	68.7	2.3	-	-	[50]
Ru-Ca/Pr_6O_{11}					60.3	2.0	-	-	
Ru-Pr/Pr_6O_{11}					67.4	2.3	-	-	
Ru-La/Pr_6O_{11}					67.4	2.3	-	-	
Ru-Gd/Pr_6O_{11}					65.4	2.2	-	-	
Ru-Cs/CeO_2-0.43	5.0	0.8	400	2,000	100	2.2	-	77.8	[46]
Ru/K-ZrO_2-KOH	4.85	0.5	350	60,000	44.3	29.6	4.9	47.2	[74]
Ru-K/MgO-CNTs	4.85				39.3	26.3	4.5	48.1	
Ru/La_2O_3-700-i-K	4.8	0.5	450	18,000	72.8	14.6	8.3	34.7	[47]
Ru-Co clusters@N-C	0.26	Co : Ru=30.0	525	12,000	22.0	2.9	1.3	-	[52]
Ru/Fe-C	0.97	Fe : Ru=2.14	600	20,000	97.5	21.7	3.3	85.6	[76]
Ru_3Fe/MWCNTs	1.98	Fe : Ru=3.02	450	6,000	81.8	5.5	1.5	-	[77]
Ru-Ni/CeO_2	2.0	Ni : Ru=5.0*	450	6,000	90.0	6.0	-	-	[38]
Ru_2La	59.3	La : Ru=2.0			46.0	9.3	-	-	
RuZr	52.6	Zr : Ru=1.0	500	18,000	38.0	7.6	-	-	[79]
Ru_2Ce	59.1	Ce : Ru=2.0			42.0	8.5	-	-	

*Weight ratio

Table 4. Fabrication of some specific Ru-based catalysts for NH₃ decomposition: comparison of different methods

Catalyst	Method	Ru content (wt%)	Ru size (nm)	$T_{reaction}$ (°C)	GHSV ($mL_{NH_3}/g_{cat.}/h$)	X_{NH_3} (%)	r_{H_2} (mmol/min/$g_{cat.}$)	TOF_{H_2} (s⁻¹)	E_{app} (kJ/mol)	Ref.
Ru/ZrO₂-imp2	WI	5.6	931.6	200	2,000	41.0	0.9	19.7	-	[83]
Ru/ZrO₂-Ipr	WI followed reduced by NaBH₄	5.3	9.3	200		62.0	1.4	0.4	-	
Ru/CeO₂-spherical	WI followed washed by aqueous ammonia	5.1	30.7	400	2,000	90.0	2.0	1.5	167	[46]
Ru/MgO-DP	DP (Urea : Ru=200 : 1)	3.5	3.3	450	36,000	54.1	21.7	3.0	83.3	[32]
Ru/MgO-IM	WI	3.5	15.8			19.3	7.7	4.7	102.7	
Ru/MgO		2.8	2.0	450	30,000	41.3	13.8	-	-	[81]
Ru/CeO₂ (nanorod)	Polyol-reduction (Ethylene glycol)		1.5			33.0	8.1	-	-	[45]
Ru/MgO		1.0	1.6	350	22,000	10.0	2.5	0.6	-	
Ru/Al₂O₃			1.7			3.5	0.8	0.2	-	
Ru/SiO₂ (Ru/Si=0.06)	One-pot hydrothermal	9.2	4-10	500	360,000	86.0	345.5	-	-	[43]
Nano-Ru@SiO₂ (core-shell) (Si/Ru=0.2)	RuO₂ capsulation	89.4	~20 (RuO₂)	450	30,000	68.5	22.9	13.8	41.2	[86]
$Sr_{0.84}Y_{0.16}$ _$Ti_{0.92}Ru_{0.08}O_{3-\delta}$ (perovskite)	Pechini method	3.98	0.97	450	10,000	56.3	0.3	-	62.8	[88]

stability than a Ru/MgO catalyst prepared by the WI method for NH₃ decomposition [32]. Through the DP process, the reduction of Ru(OH)₃ to Ru metal can happen at the low-temperature zone [85], preferring the small Ru size (high dispersion). Besides, the precipitant used in the DP process can increase the basicity of the synthesized catalyst, which is beneficial to the NH₃ decomposition.

Regarding the Ru dispersion control aspect, the polyol reduction process is applied to obtain a high Ru dispersion on mesoporous MgO [81], which exhibits high catalytic performance. By this method, almost all Ru ions could be reduced to Ruᵒ by the polyol agent in the estimated size range; therefore, the high Ru dispersion and the easy removal of Cl⁻ ions co-accelerate the decomposition of NH₃. This procedure was applied to fabricate Ru clusters stabilized on CeO₂ nanorods and it had outstanding performance (9,924 $mmol_{H2}/g_{Ru}$/min at 450 °C) [45]. Ru incorporated mesoporous silicate materials with high Ru dispersion, fabricated via the one-pot hydrothermal synthesis, was reported to be a highly efficient catalyst for NH₃ decomposition [43].

Core-shell nanostructured Ru@SiO₂, synthesized by Yao et al. [86] using an encapsulation procedure with prepared RuO₂ nanoparticles, showed superior activity and stability for NH₃ decomposition. The durable shells protect the core from aggregation and function as microcapsular-like reactors. Adsorption and catalytic reactions are enhanced in the cores. Further modification of the core surface with acid treatment, or La, Ce doping, was found to improve the catalytic activity [87]. In a separate study, Ruᵒ generated on perovskite surfaces, $Sr_{0.84}Y_{0.16}Ti_{0.92}Ru_{0.08}O_{3-\delta}$, demonstrated high-efficiency NH₃ decomposition [88] and exhibited high and stable catalytic activity at 500 °C with 10,000 $mL_{NH3}/g_{cat.}$/h of GHSV

(96% of NH₃ conversion for >275 h).

2. Ni-based Catalyst

The transitional metal Ni, one of the most common elements employed in metal-based catalysts, has been proven to catalyze the decomposition of NH₃ for H₂ production actively. Although the activity of the Ni-based catalysts is not as high as that of noble metal catalysts, they have been reported as the best performing catalysts for NH₃ decomposition among the non-noble metal-based catalysts [14,38]. The use of Ni catalysts makes it economically viable compared to noble metal catalysts. However, single component Ni catalysts cannot meet the activity and stability requirements in catalytic NH₃ decomposition. Ni dispersion, textural morphology, acidity-basicity properties, and the active metal species - support interaction are important factors that significantly influence the overall performance of Ni-based catalysts, as seen in Fig. 6. The ongoing efforts to develop novel Ni-based catalysts with excellent catalytic activity and stability for CO_x-free H₂ production have been ramped up, focusing on several approaches, including the selection of supports [60,87,89,90], the addition of promoter elements [60,87,89,90], the formation of multi-metallic compound [91-95], and the catalyst preparation method [96-99].

2-1. Supports

The electron donors from supports to active metal species can accelerate the desorption of the recombinative nitrogen atoms, which is considered a rate-limiting step in NH₃ decomposition [91], suggesting the important role of support material in this reaction. As a result, numerous developed substrates have currently been used to support Ni catalysts [100]. In general, supports that possess a high surface area, strong alkalinity, high thermal stability, and great
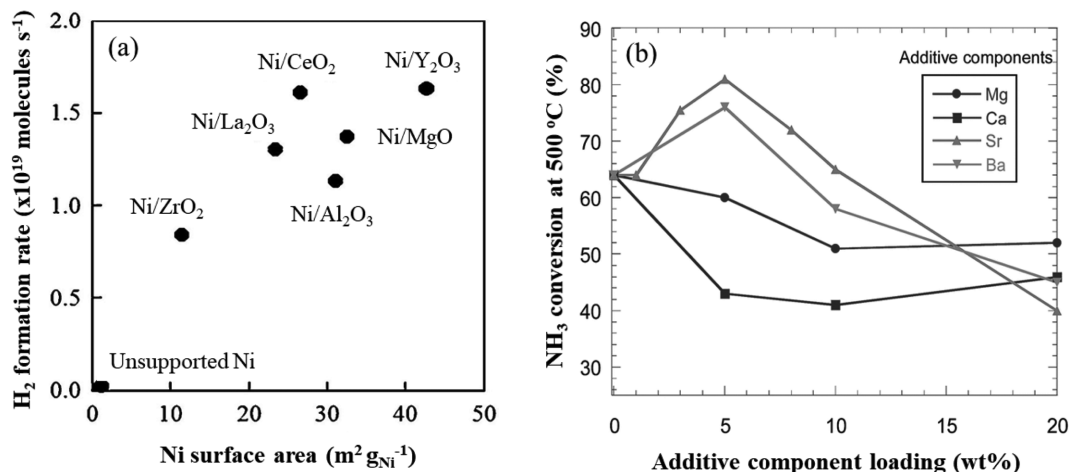
Fig. 6. (a) The H_2 formation rates via NH_3 decomposition over unsupported Ni and supported Ni catalysts as a function of the surface area of Ni (reproduced with permission from ref. [100], copyright 2016, Elsevier BV), (b) NH_3 conversion at 500 °C for 0-20 wt% additive component loading on 40 wt% Ni/Y_2O_3 (reproduced with permission from ref. [89], copyright 2016, Royal Society of Chemistry).

electron transfer capacity are preferable for the NH_3 decomposition reaction. The activity of supported Ni-based catalysts for NH_3 decomposition in recent literatures is summarized in Table 5.

Muroyama et al. [96] investigated NH_3 decomposition over Ni catalysts supported on various metal oxides (Al_2O_3, CeO_2, La_2O_3, MgO, SiO_2, TiO_2, and ZrO_2). Among these catalysts, Ni/Al_2O_3 was reported with the highest NH_3 conversion mainly because of the remarkable surface area of Al_2O_3 support (200 m^2/g). Liu et al. [98] employed the DP method to prepare a series of Ni catalysts supported on SBA-15 (Ni/SBA-15) with a small Ni particle size (4-7 nm), high Ni dispersion, and high resistance to sintering exhibiting a high NH_3 conversion efficiency and good thermal stability. The activity of these catalysts was further enriched by adding cerium or lanthanum oxides (CeNi/SBA-15 and LaNi/SBA-15) due to the improvement of Ni dispersion and the reducibility of the catalysts [101].

Despite the significantly small surface area, rare earth oxides are potential supports due to their ability to speed up recombinative hydrogen desorption, which is also known as the limiting step in NH_3 decomposition reaction catalyzed by Ni-based catalysts [13]. Research has shown that a Ni/La_2O_3 catalyst activity in the reaction was comparable to Ni/Al_2O_3, even with the relatively small surface area of the La_2O_3 support (4.7 m^2/g) [96]. Okura et al. [102] prepared various Ni catalysts supported on rare earth oxides (CeO_2, Gd_2O_3, La_2O_3, Sm_2O_3, and Y_2O_3) and tested their performance for NH_3 decomposition. The obtained results confirmed that the catalyst with a greater Ni surface provided a better activity; the highest NH_3 conversion of 87.0% was observed on Ni/Y_2O_3 at 550 °C with a GHSV of 6,000 mL/$g_{cat.}$/h. This study showed that the inhibition phenomenon of hydrogen species in the reaction would be more seriously repressed by increasing the partial pressure of hydrogen, which could be effectively alleviated with catalysts supported on most rare earth oxides. Nakamura and Fujitani [100] reported similar results where the Ni catalyst supported on Y_2O_3 showed the highest activity among those supported on other supports (Al_2O_3, CeO_2, La_2O_3, MgO, Y_2O_3, and ZrO_2). However, the

Ni-N binding energy was concluded as the main factor determining the reaction rate-limiting step, and the Ni active sites supported on different supports were not identical. As shown in Fig. 6(a), the catalyst activity in the NH_3 decomposition was determined not due to only the Ni surface area.

Moreover, Ni supported on a composite of multi rare earth metal oxides ($Ce_{0.8}Zr_{0.2}O_2$) has been reported to have good performance because of the surface area improvement of the composite and the promotional effect for hydrogen removal [103]. Furthermore, the introduction of Al into the $Ce_{0.8}Zr_{0.2}O_2$ structure produced more surface oxygen vacancies, leading to a superior catalytic activity of Ni/Al-$Ce_{0.8}Zr_{0.2}O_2$ [57]. The promotional effects of surface oxygen vacancies have also been verified in the recent literature [55,60] and will be discussed in the following sections.

Natural clay supported Ni catalysts have also been investigated recently. Mica (MS), a porous natural layered mineral with high thermal stability, has also been investigated as support for NH_3 decomposition by Hu et al. [104]. In that study, the uniform dispersion of the Ni species on the MS layered structure is responsible for the high performance of the resulting catalysts. Moreover, Ni catalysts supported on natural porous attapulgite (ATP) clay (fibrillar hydrated magnesium aluminum silicate) and that encapsulated with porous silica to form a core-shell structure have shown a higher specific activity and stability than its counterparts [44]. More recently, sepiolite (Sp) clay (hydrous magnesium silicate) with a high surface area and strong basic character has also been demonstrated as effective support for Ni catalysts in NH_3 decomposition [14].

LDHs generally consist of positively charged mixed metal hydroxide layers and exchangeable charge-balancing interlayer anions, exhibiting versatile physicochemical properties [105]. Su et al. [105] introduced Ni catalysts into MgAl-LDHs via hydrothermal treatment method, and the resulting NiMgAl-LDHs composite shows a superior catalytic activity and thermal stability for NH_3 decomposition. This outstanding catalytic activity of the NiMgAl-LDHs could be credited for the oxide matrix's synergy and the Ni-Mg

Table 5. Catalytic activity of the supported Ni catalysts for NH₃ decomposition

Catalyst	Ni content (wt%)	$T_{reaction}$ (°C)	GHSV ($mL_{NH_3}/g_{cat.}$/h)	X_{NH_3} (%)	r_{H_2} (mmol/min/$g_{cat.}$)	TOF_{H_2} (s⁻¹)	E_{app} (kJ/mol)	Ref.
Ni/SBA-15	23.4	600	46,000	96.2	32.2	0.67	-	[98]
Ni/TiO₂				30.0	2.0	-	-	
Ni/BaTiO₃				75.0	5.0	-	-	
Ni/SrTiO₃				80.0	5.4	-	-	
Ni/CaTiO₃				37.0	2.5	-	-	
Ni/ZrO₂	40	550	6,000	27.0	1.8	-	-	[13]
Ni/BaZrO₃				94.0	6.3	-	-	
Ni/SrZrO₃				90.0	6.0	-	-	
Ni/CaZrO₃				50.0	3.3	-	-	
Ni/Al₂O₃	8.9			27.0	2.7	0.39	91.5	
Ni/Ce₀.₈Zr₀.₂O₂	10.7	500	9,000	48.0	4.8	0.34	73.8	[57]
Ni/Al-Ce₀.₈Zr₀.₂O₂	8.0			58.0	5.9	0.48	66.8	
Ni/SiO₂	5	600	30,000	53.7	18.8	-	-	[42]
Ni/Al₂O₃	9	450	6,000	10.0	0.7	0.22	-	[60]
Ni/Al₂O₃	10	450	9,500ᵃ	60	0.4	-	-	[122]
Ni/Y₂O₃	40	500	6,000	64.0	4.3	-	-	[89]
Ni/Sepiolite	5.2	650	8,300	99.2	9.2	-	-	[14]
Ni/Mica	15.0	650	30,000	97.2	32.5	-	-	[104]
Ni-10/ATP	8.2	650	30,000	64.3	21.5	-	75.2	[44]
Ni-30/ATP@SiO₂	8.7			73.4	24.6	-	80.1	
Ni₁.₂₆(Al₀.₃Oₙ)	71.4	600	30,000	80.1	26.8	0.40ᵇ	-	[105]
Ni₀.₆(Mg₀.₂₉Al₀.₅₇Oₙ)	40.1			99.3	33.3	0.70ᵇ	-	
Ni₁/C-LDHs-ST	23.6	600	10,000	98.8	11.0	-	-	[106]
Ni/AC	5	500	6,000	24.8	1.7	-	-	[107]
Ni/MWCNT				57.6	3.9	-	-	
Ni/AC				40.9	13.7	-	-	
Ni/rGO	10	700	30,000	81.9	27.4	-	65.3	[108]
Ni/OMC				56.8	19.0	-	-	
Ni/Al₂O₃				70.0	4.7	-	-	
Ni/La₂O₃				62.0	4.2	-	-	
Ni/CeO₂	10	550	6,000	24.0	1.6	-	-	[102]
Ni/Sm₂O₃				80.0	5.4	-	-	
Ni/Gd₂O₃				80.0	5.4	-	-	
Ni/Y₂O₃				87.0	5.8	-	-	
Ni/MRM	12	700	30,000	95.5	32.0	-	72.1	[116]
Ni/La₂O₃	10	550	30,000	59	19.8	1.6ᶜ	53.9	[48]
Ni/MgLa	40			82	27.5	-	-	

ᵃ5.9% NH₃-Ar

ᵇData calculated at 550 °C

ᶜData calculated at 350 °C

sites. Similar results can be found in Zhao et al. [106], in which the Ni catalysts were strongly and evenly interlaced on the brucite-like layers of the hydrocalumite-LDHs through a structure-transformation process. The obtained catalysts provided a higher number of B₅ sites, which can enhance the hydrogen spillover effect, and thus an excellent activity for NH₃ decomposition can be expected [106].

Regarding the carbon support materials, Ni supported on MWCNTs can provide better catalytic performance than that supported on AC, although MWCNTs or AC has no substantial effect

Table 6. Catalytic activity of the promoted Ni-based catalysts, catalysts with multi-active sites, and alloy catalysts included Ni for NH$_3$ decomposition

Catalyst	Ni content (wt%)	Promoter content (wt%)/active metal molar ratio	$T_{reaction}$ (°C)	GHSV (mL$_{NH_3}$/g$_{cat.}$·h)	X_{NH_3} (%)	r_{H_2} (mmol/min/g$_{cat.}$)	TOF$_{H_2}$ (s^{-1})	Ref.
K-Ni/SiO$_2$	5	K : Ni=2	600	30,000	62.0	20.8	-	[42]
Y-Ni/Al$_2$O$_3$					18.8	1.3	0.38	
La-Ni/Al$_2$O$_3$					20.2	1.4	0.38	
Ce-Ni/Al$_2$O$_3$					15.4	1.0	0.29	
Pr-Ni/Al$_2$O$_3$	10	12	450	6,000	19.7	1.3	0.43	[60]
Nd-Ni/Al$_2$O$_3$					19.7	1.3	0.37	
Sm-Ni/Al$_2$O$_3$					18.2	1.2	0.38	
Eu-Ni/Al$_2$O$_3$					15.9	1.1	0.31	
Gd-Ni/Al$_2$O$_3$					15.8	1.1	0.31	
Mg-Ni/Y$_2$O$_3$					60.0	4.0	-	
Ca-Ni/Y$_2$O$_3$	40	5	500	6,000	43.0	2.9	-	[89]
Sr-Ni/Y$_2$O$_3$					81.0	5.4	-	
Ba-Ni/Y$_2$O$_3$					76.0	5.1	-	
Ir-Ni/Al$_2$O$_3$	10	0.7	450	9,500[a]	76.6	0.5	-	[122]
Fe-Ni/Al$_2$O$_3$	10[b]	Ni : Fe=0.2	650	28,500	99.7	31.7	-	[93]
Ni-Co/SiO$_2$	10[b]	Ni : Co=1.0	550	30,000	76.8	25.7	-	[94]
NiMoN	23.0	Ni : Mo=0.8	650	21,600	100	24.1	-	[99]
Ni$_3$Mo$_3$N	36.8	Ni : Mo=1.0	550	6,000	83	5.6	-	[114]
Fe$_{10}$Ni$_{10}$Cu$_{10}$Co$_{55}$Mo$_{15}$/CNF	9.3[b]	-	500	36,000	100	40.2	7.0	[95]
Ni-Fe/SiO$_2$	10[b]	Ni : Fe=0.7	500	14,400	99.9	16.0	-	[112][c]
Ni-Co/CZY	10[b]	-	600	6,000	100	-	-	[113]
Ni-Al alloy	80.1[b]	-	500	30,000	43.0	14.4	-	[117]

[a]5.90% NH$_3$-Ar

[b]Total weight percentage of active metal

[c]Plasma-assisted

on the Ni phase configuration of the catalysts. Therefore, the better catalytic performance of Ni/MWCNTs could be attributed to the synergistic effect of Ni-support interaction and the unique electronic property of the MWCNTs [107]. Meng et al. [108] utilized reduced graphene oxide (rGO) as a support for Ni catalyst, which could enhance the catalytic performance of NH$_3$ decomposition compared to AC supports because of highly Ni dispersion and the conductivity of the graphene. NH$_3$ conversion of 81.9% and H$_2$ generation rate of 1.64 mol/g$_{cat.}$/h have been reported over 10 wt%Ni/rGO at 700 °C with a GHSV 30,000 mL/g$_{cat.}$/h [108].

2-2. Promoted Catalysts, Multi-active Sites, and Alloy Catalysts

Alkali, alkaline earth, or rare earth metals have been widely used to integrate with Ni-based catalysts for enhancing their catalytic performance in NH$_3$ decomposition [13,60,89]. The integration of these elements is expected to modify the morphology, electronic state of Ni active sites or decrease the binding energy between Ni species and N atoms due to their electron-donating character, and consequently enhance the performance of the prepared catalysts [42,60,89,90,109]. Im et al. [109] studied the influence of the basicity of catalyst in NH$_3$ decomposition reaction catalyzed by various

Ni catalysts supported on alkaline earth metal aluminate compounds. They suggested that the catalysts with strong basicity are beneficial in alleviating the H$_2$ inhibition effect by reducing the H$_2$ desorption energy, and the NH$_3$ conversion increased when increasing the basic strength in the order of Ni/Mg-Al-O<Ni/Ca-Al-O<Ni/Sr-Al-O<Ni/Ba-Al-O. Table 6 shows the effects of various promoters in NH$_3$ decomposition reaction catalyzed by the corresponded Ni-based catalysts, the multi-active sites catalysts, and alloy catalysts included Ni.

Alkali metal, specifically K, has not shown a significant effect on the performance of Ni catalysts supported on MCM-41, SBA-15, and SiO$_2$, which has been reported in a study by Li et al. [42]. Okura et al. [89] reported on the different effects of additive alkaline earth metals on Ni/Y$_2$O$_3$ catalyst, in which a small amount of Sr or Ba addition can significantly accelerate the activity of the catalyst, while the presence of Ca and Mg was not effective for this reaction (Fig. 6(b)). The promotion effect of Sr and Ba addition was explained by enhancing the electron density in the Ni metal and the strong Ni-Sr, Ni-Ba interaction [89]. The addition of La over Ni/Al$_2$O$_3$ system was beneficial to the catalytic performance

[17,60,110]. This modification impacted the morphological and electronic properties of catalysts that could alter the local arrangement of Ni species and maximizes the number of Ni stepped sites. Besides, additive La could minimize the Ni active size and reduce the stability of reaction intermediates over active sites, thus increasing the decomposition rate [17]. Another beneficial effect of La is promoting larger open mesopores and higher Ni dispersion [110].

A similar promotion effect was also reported from the addition of Ce, which significantly accelerated the low-temperature activity of the Ni/Al$_2$O$_3$ catalyst [56,60,111]. Zhang et al. [87] prepared a core-shell structure of Ce-doped NiO nanoparticles encapsulated in SiO$_2$ (Ce-NiO@SiO$_2$), which proved to be effective for NH$_3$ decomposition. The addition of a suitable amount of Ce could promote the high Ni dispersion, providing better catalytic activity than that with no additive. Moreover, the SiO$_2$ shell can effectively protect the active phase from sintering, making it highly stable at high reaction temperature. In addition, mesoporous multi-metal oxide microspheres with a tricomponent of Ni-Ce-Al-O prepared by an aerosol-assisted self-assembly method exhibited significant improvement than to pure NiO or bicomponent catalysts [55], suggesting the synergistic effect between Ce and Al promotes the Ni catalyst activity.

Ni-based catalysts with multi-active sites can possess distinct physicochemical and electronic properties from their counter metals [93,94,99,112-114], enhancing the NH$_3$ decomposition efficiency (Table 6). Simonsen et al. [92] developed alloyed Ni-Fe/Al$_2$O$_3$ catalysts and tested for NH$_3$ decomposition corresponding to several parameters, including Ni-Fe ratio, oxide support phase, and type of Ni-Fe alloy phase. The alloyed Ni-Fe supported on Al$_2$O$_3$ exhib-ited a significant enhancement in catalytic activity compared to that of the single Ni or Fe supported on Al$_2$O$_3$. The authors also suggested that the small Ni-Fe size is very important to obtain a high NH$_3$ conversion because of a large active surface area and a structural effect. Additionally, Al$_2$O$_3$ or Mg-Al-spinel are preferable support materials compared to SiO$_2$, TiO$_2$, and ZrO$_2$, for which the small size of the Ni-Fe nanoparticles is challenging to obtain at a high-temperature range. More recently, a new class of catalysts called high-entropy alloys (HEA), made of earth-abundant metals (Fe, Ni, Cu, Co, and Mo), have been reported by Xie et al. [95]. These catalysts showed excellent catalytic activity and stability in NH$_3$ decomposition reaction, with over 20 times enhancement factors of activity than the precious metal Ru. However, the harsh synthetic conditions of the HEA may hinder their practical application.

2-3. Synthetic Methods

The catalyst preparation method is another important factor affecting the catalytic performance of the obtained catalysts by changing their physicochemical properties, and numerous synthetic approaches have been proposed for the preparation of highly active and stable Ni-based catalysts [96,97]. Traditional synthetic methods (co-precipitation (CP), DP, and WI methods) are widely used to prepare Ni-based catalysts in the current literature and generally suffer from the low stability due to thermal sintering of the Ni species at high reaction temperature. The CP method can provide narrow size distribution of catalysts, but it is difficult to control and reproduce, whereas the desired active phase distribution, loading, and/or dispersion may not always be given by the WI method [98].

Table 7. Fabrication of some specific Ni-based catalysts for NH₃ decomposition: comparison of different methods

Catalysts	Method	Ni dispersion (%)	Ni content (wt%)	T$_{reaction}$ (°C)	GHSV (mL$_{NH_3}$/g$_{cat.}$·h)	X$_{NH_3}$ (%)	r$_{H_2}$ (mmol/min/g$_{cat.}$)	TOF$_{H_2}$ (s⁻¹)	E$_{app}$ (kJ/mol)	Ref.
Ni/La$_2$O$_3$	WI	-				74.0	4.96	-	-	
Ni/La$_2$O$_3$	CAC	-				76.0	5.09	-	-	
Ni/La$_2$O$_3$	NH$_3$-CP	-	26.5	550	6,000	66.0	4.42	-	-	[96]
Ni/La$_2$O$_3$	NaOH-CP	-				69.0	4.62	-	-	
Ni/La$_2$O$_3$	PR	-				59.0	3.95	-	-	
Ni/SBA-15	WI	0.9 (100)	10	550	30,000	50.8	17.0	18.48	-	[98]
Ni/SBA-15	DP	>20 (5)	23.4			89.0	29.8	0.62	-	
Ni/MCM-41	WI	-	5			64.2	21.5	-	-	
Ni/MCM-41	TIE	-	7.2	600	30,000	71.6	24.0	-	-	[42]
K-Ni/MCM-41	WI	9.9	5			65.1	21.8	4.3	53.5	
K-Ni-MCM-41	TIE	14.4	7.2			73.2	24.5	2.4	49.3	
Ni/ZSM	IM	-				50.1	16.8	-	98.2	
Ni/ZSM	DP	-	5	650	30,000	81.3	27.2	-	98.1	[97]
Ni/ZSM	SSIE	-				92.9	31.1	-	97.7	
Ni/ZSM	MSSIE	-				97.6	32.7	-	88.1	
Ni-Mo nitride	Acetate-EVP	-	23.0			83.0	20.0	-	-	
Ni-Mo nitride	Acetate-CP	-	20.7	550	21,600	39.0	9.4	-	-	[99]
Ni-Mo nitride	Nitrate-EVP	-	12.6			52.0	12.5	-	-	
Ni-Mo nitride	Nitrate-CP	-	19.9			75.0	18.1	-	-	

*Data in the parentheses refer to Ni size in nm.

As seen in Table 7, the Ni/La$_2$O$_3$ catalyst prepared by the citric acid complex (CAC) method or WI method was observed with a higher NH$_3$ conversion than those prepared by NH$_3$ co-precipitation (NH$_3$-CP), NaOH co-precipitation (NaOH-CP), or the pyrolysis (PR) method [96]. Hu et al. [97] published a comparative study of various catalyst fabrication techniques, including WI, DP, solid-state ion exchange (SSIE), and modified solid-state ion exchange (MSSIE) methods, for a series of Ni catalysts supported on zeolite ZSM-5 (Ni/ZSM-5). The results indicated that preparation methods could affect the Ni metal species dispersion and their catalytic activity in the NH$_3$ decomposition reaction. Among the resulting catalysts, the Ni/ZSM-5 prepared by the MSSIE method exhibited the best catalytic performance with the lowest E$_{app}$ because of the highly dispersed and small size of Ni species, strong SMSI, and suitable acidity [97]. A Ni catalyst supported on MCM-41 prepared by the template-ion exchange (TIE) technique was reported with a larger Ni positioned inside the pores and a better Ni dispersion on the support. Consequently, it provided better catalytic performance in NH$_3$ decomposition reaction than that prepared by the WI method [42]. Leybo et al. [99] elucidated the influence of the initial salt composition (acetate and nitrate) and the precursor production method (evaporation (EVP) and CP) on the composition, morphology, and performance of the multi-active sites NiMoN catalysts. It was determined that the larger specific surface area and the higher Ni$_2$Mo$_3$N phase content in the obtained catalysts resulted in a higher NH$_3$ conversion, which increased in the order of NiMoN-nitrate-EVP<NiMoN-acetate-CP<NiMoN-nitrate-CP<NiMoN-acetate-EVP.

The synthesis conditions of the selected method are also very important in determining the reactivity of the obtained catalysts. For instance, the calcination temperature can alter the dispersion of active metal nanoparticles, thereby affecting their catalytic activity. Haynes et al. [115] reported on the changes in structure and activity of Ni-based lanthanum zirconate pyrochlore catalysts according to the calcination temperature (700-1,000 °C), for which the material calcined at low temperatures can provide higher activity and selectivity for NH$_3$ decomposition. This result was explained by the formation of smaller and well-dispersed Ni species and a smaller amount of La enrichment at the surface when calcination is performed at a low temperature. Yu et al. [48] revealed that La$_2$O$_3$ calcined at 450 °C much better than in the range of 550-850 °C when supported to Ni; it possessed the highest specific surface area and surface oxygen concentration. The Ni content effects have also been broadly investigated in the range of 1-60 wt% on various supports [48,97,102,104,108,116,117]. In terms of the NH$_3$ conversion, the optimal Ni loading was proposed as 40 wt% on Y$_2$O$_3$ support [102] and the 5MgLa (5 : 1 molar ratio) support [48], as 15 wt% on the mica support [104], as 12 wt% on the modified-red-mud (MRM) support [116], as 10 wt% on the rGO support [108], and as 5 wt% on the support ZSM-5 prepared by the MSSIE method [97].

Recently, many attempts have been made to develop new fabrication processes for highly active Ni-based catalysts. In this respect, a lower-temperature chemical alloying (LTCA) technique has been used to prepare Ni-Al alloy powders, converted into porous Ni catalysts by a post-Al leaching step in a study by Lee et al. [117].

The skeletal Ni catalysts possess a high BET surface and high reactivity toward NH$_3$ decomposition than the commercial Raney Ni powder. The LTCA method has appeared to be more cost-effective than the commercial Raney-Ni-precursor fabrication method since it does not necessarily need high temperature and strenuous pulverization processes. Ni impregnated on 3D-printed CeO$_2$ structures exhibited excellent catalytic performance for NH$_3$ decomposition in a study by Lucentini et al. [118], where CeO$_2$ 3D-printing was reported for the first time. The proposed method could offer new and exciting perspectives to prepare customized CeO$_2$-based catalytic structures with various geometries, bringing a significant improvement of the catalytic performance in NH$_3$ decomposition reaction.

SUMMARY AND OUTLOOK

The core issue in developing NH$_3$ decomposition catalysts involves accelerating the rate-controlling step, mainly dependent on Ru-N and Ni-N bonding strength. A moderate bonding strength can benefit the dissociation of the N-H bond and favor strong desorption of N (ad), while a weak or strong bonding strength promotes only one side of the reaction. Therefore, it is necessary to develop new materials and new catalyst preparation methods to help newly designed catalysts achieve efficient NH$_3$ decomposition. This review has summarized the recent developments of Ru- and Ni-based materials as a contribution to developing efficient NH$_3$ decomposition catalysts. Almost all the results here imply that electron-conductive supports could promote a highly efficient Ru- or Ni-based catalyst for NH$_3$ decomposition with strong basicity. Basicity has an essential role in electron enrichment for active sites, leading to recombinative N$_2$ desorption. However, the development of NH$_3$ decomposition catalysts still faces challenges.

First, the universal control of active metal shapes and sizes can maximize the number of reactive sites. The investigations into various alloy structures have indicated great potential for implementing NH$_3$ decomposition catalysts in practical systems under various reaction conditions. Besides, the addition of suitable promoters by the optimum loading order is an effective way to NH$_3$ conversion enhancement.

Second, the development of new materials or the modification of available supports helps control the particle size to increase the dispersion of active metals, e.g., graphene nanocomposites, high surface area graphite, CNFs, and MOFs. Recently, a new research area in NH$_3$ decomposition explored the combination of Ru, Ni, and amide; however, improving their stability is still a challenge. The optimum combined structure of those compounds can further support Ru or Ni to achieve outstanding catalytic performance.

Third, the proper fabrication method should be innovated, which corresponds to each precursor of NH$_3$ decomposition catalysts to ensure high dispersion, a well-designed structure, and sufficient SMSI for long-term stability retaining their practical applicability.

ACKNOWLEDGEMENTS

30) from the Korea Research Institute of Chemical Technology (KRICT).

REFERENCES

1. I. Staffell, D. Scamman, A. V. Abad, P. Balcombe, P. E. Dodds, P. Ekins, N. Shah and K. R. Ward, *Energy Environ. Sci.*, **12**, 463 (2019).
2. X. C. S. Rivera, E. Topriska, M. Kolokotroni and A. Azapagic, *J. Cleaner Prod.*, **196**, 863 (2018).
3. R. Zeng, M. Feller, Y. Ben-David and D. Milstein, *J. Am. Chem. Soc.*, **139**, 5720 (2017).
4. W. J. Lee, C. Li, H. Prajitno, J. Yoo, J. Patel, Y. Yang and S. Lim, *Catal. Today*, In press (2020).
5. S. F. Yin, B. Q. Xu, X. P. Zhou and C. T. Au, *Appl. Catal. A*, **277**, 1 (2004).
6. E. García-Bordejé, S. Armenise and L. Roldán, *Catal. Rev.*, **56**, 220 (2014).
7. A. Klerke, C. H. Christensen, J. K. Nørskov and T. Vegge, *J. Mater. Chem.*, **18**, 2304 (2008).
8. J. Andersson and S. Grönkvist, *Int. J. Hydrogen Energy*, **44**, 11901 (2019).
9. K. E. Lamb, M. D. Dolan and D. F. Kennedy, *Int. J. Hydrogen Energy*, **44**, 3580 (2019).
10. A. K. Hill and L. Torrente-Murciano, *Appl. Catal. B*, **172-173**, 129 (2015).
11. S. Mukherjee, S. V. Devaguptapu, A. Sviripa, C. R. F. Lund and G. Wu, *Appl. Catal. B*, **226**, 162 (2018).
12. T. E. Bell, G. Zhan, K. Wu, H. C. Zeng and L. Torrente-Murciano, *Top. Catal.*, **60**, 1251 (2017).
13. K. Okura, K. Miyazaki, H. Muroyama, T. Matsui and K. Eguchi, *RSC Adv.*, **8**, 32102 (2018).
14. S. F. Kurtoğlu, S. Sarp, C. Y. Akkaya, B. Yağcı, A. Motallebzadeh, S. Soyer-Uzun and A. Uzun, *Int. J. Hydrogen Energy*, **43**, 9954 (2018).
15. T. E. Bell and L. Torrente-Murciano, *Top. Catal.*, **59**, 1438 (2016).
16. M. C. J. Bradford, P. E. Fanning and M. A. Vannice, *J. Catal.*, **172**, 479 (1997).
17. J. Zhang, H. Xu and W. Li, *Appl. Catal. A*, **296**, 257 (2005).
18. A. Takahashi and T. Fujitani, *J. Chem. Eng. Japan*, **49**, 22 (2016).
19. C. Egawa, T. Nishida, S. Naito and K. Tamaru, *J. Chem. Soc., Faraday Trans. 1 F*, **80**, 1595 (1984).
20. W. Tsai and W. H. Weinberg, *J. Phys. Chem.*, **91**, 5302 (1987).
21. H. Dietrich, K. Jacobi and G. Ertl, *Surf. Sci.*, **352-354**, 138 (1996).
22. A. Boisen, S. Dahl, J. K. Nørskov and C. H. Christensen, *J. Catal.*, **230**, 309 (2005).
23. C. J. H. Jacobsen, S. Dahl, B. S. Clausen, S. Bahn, A. Logadottir and J. K. Nørskov, *J. Am. Chem. Soc.*, **123**, 8404 (2001).
24. D. A. Hansgen, D. G. Vlachos and J. G. Chen, *Nat. Chem.*, **2**, 484 (2010).
25. J. C. Ganley, F. S. Thomas, E. G. Seebauer and R. I. Masel, *Catal. Lett.*, **96**, 117 (2004).
26. W. Zheng, J. Zhang, H. Xu and W. Li, *Catal. Lett.*, **119**, 311 (2007).
27. A. M. Karim, V. Prasad, G. Mpourmpakis, W. W. Lonergan, A. I. Frenkel, J. G. Chen and D. G. Vlachos, *J. Am. Chem. Soc.*, **131**, 12230 (2009).
28. F. R. García-García, A. Guerrero-Ruiz and I. Rodríguez-Ramos,

Top. Catal., **52**, 758 (2009).
29. X. Duan, G. Qian, Y. Liu, J. Ji, X. Zhou, D. Chen and W. Yuan, *Fuel Process. Technol.*, **108**, 112 (2013).
30. S. Chen, X. Chen and H. Zhang, *Int. J. Hydrogen Energy*, **42**, 17122 (2017).
31. X. Ju, L. Liu, X. Zhang, J. Feng, T. He and P. Chen, *ChemCatChem*, **11**, 4161 (2019).
32. X. Ju, L. Liu, P. Yu, J. Guo, X. Zhang, T. He, G. Wu and P. Chen, *Appl. Catal. B*, **211**, 167 (2017).
33. Y. Ogura, K. Sato, S.-i. Miyahara, Y. Kawano, T. Toriyama, T. Yamamoto, S. Matsumura, S. Hosokawa and K. Nagaoka, *Chem. Sci.*, **9**, 2230 (2018).
34. S. J. Wang, S. F. Yin, L. Li, B. Q. Xu, C. F. Ng and C. T. Au, *Appl. Catal. B*, **52**, 287 (2004).
35. W. Han, Z. Li and H. Liu, *J. Rare Earths*, **37**, 492 (2019).
36. L. Li, Y. Wang, Z. P. Xu and Z. Zhu, *Appl. Catal. A*, **467**, 246 (2013).
37. L. H. Yao, Y. X. Li, J. Zhao, W. J. Ji and C. T. Au, *Catal. Today*, **158**, 401 (2010).
38. I. Lucentini, A. Casanovas and J. Llorca, *Int. J. Hydrogen Energy*, **44**, 12693 (2019).
39. Z. Wang, Z. Cai and Z. Wei, *ACS Sustainable Chem. Eng.*, **7**, 8226 (2019).
40. B. Lorenzut, T. Montini, C. C. Pavel, M. Comotti, F. Vizza, C. Bianchini and P. Fornasiero, *ChemCatChem*, **2**, 1096 (2010).
41. Z. Wang, Y. Qu, X. Shen and Z. Cai, *Int. J. Hydrogen Energy*, **44**, 7300 (2019).
42. X.-K. Li, W.-J. Ji, J. Zhao, S.-J. Wang and C.-T. Au, *J. Catal.*, **236**, 181 (2005).
43. D. Varisli and E. E. Elverisli, *Int. J. Hydrogen Energy*, **39**, 10399 (2014).
44. P. Yu, J. Guo, L. Liu, P. Wang, F. Chang, H. Wang, X. Ju and P. Chen, *J. Phys. Chem. C*, **120**, 2822 (2016).
45. X.-C. Hu, X.-P. Fu, W.-W. Wang, X. Wang, K. Wu, R. Si, C. Ma, C.-J. Jia and C.-H. Yan, *Appl. Catal. B*, **268**, 118424 (2020).
46. T. Furusawa, H. Kuribara, K. Kimura, T. Sato and N. Itoh, *Ind. Eng. Chem. Res.*, **59**, 18460 (2020).
47. C. Huang, Y. Yu, J. Yang, Y. Yan, D. Wang, F. Hu, X. Wang, R. Zhang and G. Feng, *Appl. Surf. Sci.*, **476**, 928 (2019).
48. Y. Yu, Y.-M. Gan, C. Huang, Z.-H. Lu, X. Wang, R. Zhang and G. Feng, *Int. J. Hydrogen Energy*, **45**, 16528 (2020).
49. K. Nagaoka, K. Honda, M. Ibuki, K. Sato and Y. Takita, *Chem. Lett.*, **39**, 918 (2010).
50. K. Nagaoka, T. Eboshi, N. Abe, S.-i. Miyahara, K. Honda and K. Sato, *Int. J. Hydrogen Energy*, **39**, 20731 (2014).
51. L. Li, Z. H. Zhu, Z. F. Yan, G. Q. Lu and L. Rintoul, *Appl. Catal. A*, **320**, 166 (2007).
52. J. Yang, D. He, W. Chen, W. Zhu, H. Zhang, S. Ren, X. Wang, Q. Yang, Y. Wu and Y. Li, *ACS Appl. Mater. Interfaces*, **9**, 39450 (2017).
53. X. Duan, J. Zhou, G. Qian, P. Li, X. Zhou and D. Chen, *Chin. J. Catal.*, **31**, 979 (2010).
54. J. Zhao, S. Xu, H. Wu, Z. You, L. Deng and X. Qiu, *Chem. Commun.*, **55**, 14410 (2019).
55. H. Yan, Y.-J. Xu, Y.-Q. Gu, H. Li, X. Wang, Z. Jin, S. Shi, R. Si, C.-J. Jia and C.-H. Yan, *J. Phys. Chem. C*, **120**, 7685 (2016).
56. W. Zheng, J. Zhang, Q. Ge, H. Xu and W. Li, *Appl. Catal. B*, **80**, 98 (2008).
57. D. Sima, H. Wu, K. Tian, S. Xie, J. J. Foo, S. Li, D. Wang, Y. Ye, Z.

Zheng and Y.-Q. Liu, *Int. J. Hydrogen Energy*, **45**, 9342 (2020).

58. S. Podila, H. Driss, S. F. Zaman, Y. A. Alhamed, A. A. AlZahrani, M. A. Daous and L. A. Petrov, *J. Mol. Catal. A: Chem.*, **414**, 130 (2016).

59. S. Podila, H. Driss, S. F. Zaman, A. M. Ali, A. A. Al-Zahrani, M. A. Daous and L. A. Petrov, *Int. J. Hydrogen Energy*, **42**, 24213 (2017).

60. K. Okura, T. Okanishi, H. Muroyama, T. Matsui and K. Eguchi, *Appl. Catal. A*, **505**, 77 (2015).

61. T. A. Le, Y. Kim, H. W. Kim, S.-U. Lee, J.-R. Kim, T.-W. Kim, Y.-J. Lee and H.-J. Chae, *Appl. Catal. B*, **285**, 119831 (2021).

62. F. Hayashi, Y. Toda, Y. Kanie, M. Kitano, Y. Inoue, T. Yokoyama, M. Hara and H. Hosono, *Chem. Sci.*, **4**, 3124 (2013).

63. J. Cha, T. Lee, Y.-J. Lee, H. Jeong, Y. S. Jo, Y. Kim, S. W. Nam, J. Han, K. B. Lee, C. W. Yoon and H. Sohn, *Appl. Catal. B*, **283**, 119627 (2021).

64. L. Wang, J. Chen, L. Ge, Z. Zhu and V. Rudolph, *Energy Fuels*, **25**, 3408 (2011).

65. W. Gao, J. Guo and P. Chen, *Chin. J. Chem.*, **37**, 442 (2019).

66. Z. Hu, J. Mahin and L. Torrente-Murciano, *Int. J. Hydrogen Energy*, **44**, 30108 (2019).

67. F. R. García-García, A. Guerrero-Ruiz, I. Rodríguez-Ramos, A. Goguet, S. O. Shekhtman and C. Hardacre, *Phys. Chem. Chem. Phys.*, **13**, 12892 (2011).

68. S. Sayas, N. Morlanés, S. P. Katikaneni, A. Harale, B. Solami and J. Gascon, *Catal. Sci. Technol.*, **10**, 5027 (2020).

69. T. W. Hansen, J. B. Wagner, P. L. Hansen, S. Dahl, H. Topsøe and C. J. H. Jacobsen, *Science*, **294**, 1508 (2001).

70. W. Raróg-Pilecka, D. Szmigiel, Z. Kowalczyk, S. Jodzis and J. Zielinski, *J. Catal.*, **218**, 465 (2003).

71. L. Li, Z. H. Zhu, G. Q. Lu, Z. F. Yan and S. Z. Qiao, *Carbon*, **45**, 11 (2007).

72. S.-F. Yin, B.-Q. Xu, C.-F. Ng and C.-T. Au, *Appl. Catal. B*, **48**, 237 (2004).

73. D. Szmigiel, W. Raróg-Pilecka, E. Miśkiewicz, Z. Kaszkur and Z. Kowalczyk, *Appl. Catal. A*, **264**, 59 (2004).

74. S.-F. Yin, B.-Q. Xu, S.-J. Wang and C.-T. Au, *Appl. Catal. A*, **301**, 202 (2006).

75. M. Miyamoto, A. Hamajima, Y. Oumi and S. Uemiya, *Int. J. Hydrogen Energy*, **43**, 730 (2018).

76. L. Li, F. Chen, Y. Dai, J. Wu, J. L. Shao and H. Y. Li, *RSC Adv.*, **6**, 102336 (2016).

77. C. Chen, Y. Chen, A. M. Ali, W. Luo, J. Wen, L. Zhang and H. Zhang, *Chem. Eng. Technol.*, **43**, 719 (2020).

78. X. Chen, J. Zhou, S. Chen and H. Zhang, *J. Nanopart. Res.*, **20**, 148 (2018).

79. S. Furukawa, A. Tsuchiya, Y. Kojima, M. Endo and T. Komatsu, *Chem. Lett.*, **45**, 158 (2016).

80. L. Torrente-Murciano, *J. Nanopart. Res.*, **18**, 87 (2016).

81. J. Zhang, H. Xu, Q. Ge and W. Li, *Catal. Commun.*, **7**, 148 (2006).

82. Z. Hu, J. Mahin, S. Datta, T. E. Bell and L. Torrente-Murciano, *Top. Catal.*, **62**, 1169 (2019).

83. T. Furusawa, M. Shirasu, K. Sugiyama, T. Sato, N. Itoh and N. Suzuki, *Ind. Eng. Chem. Res.*, **55**, 12742 (2016).

84. S.-F. Yin, Q.-H. Zhang, B.-Q. Xu, W.-X. Zhu, C.-F. Ng and C.-T. Au, *J. Catal.*, **224**, 384 (2004).

85. N. Abudukelimu, H. Xi, Z. Gao, Y. Zhang and Y. Ma, *Mater. Sci.*

Eng. Adv. Res., **1**, 31 (2015).

86. L. Yao, T. Shi, Y. Li, J. Zhao, W. Ji and C.-T. Au, *Catal. Today*, **164**, 112 (2011).

87. L.-F. Zhang, M. Li, T.-Z. Ren, X. Liu and Z.-Y. Yuan, *Int. J. Hydrogen Energy*, **40**, 2648 (2015).

88. H. Doh, H. Y. Kim, G. S. Kim, J. Cha, H. S. Park, H. C. Ham, S. P. Yoon, J. Han, S. W. Nam, K. H. Song and C. W. Yoon, *ACS Sustainable Chem. Eng.*, **5**, 9370 (2017).

89. K. Okura, T. Okanishi, H. Muroyama, T. Matsui and K. Eguchi, *RSC Adv.*, **6**, 85142 (2016).

90. S. Henpraserttae, S. Charojrochkul, L. Lawtrakul and P. Toochinda, *ChemistrySelect*, **3**, 11842 (2018).

91. N. Shimoda, R. Yoshimura, T. Nukui and S. Satokawa, *J. Chem. Eng. Japan*, **52**, 10 (2019).

92. S. B. Simonsen, D. Chakraborty, I. Chorkendorff and S. Dahl, *Appl. Catal. A*, **447-448**, 22 (2012).

93. H. Silva, M. G. Nielsen, E. M. Fiordaliso, C. D. Damsgaard, C. Gundlach, T. Kasama, I. b. Chorkendorff and D. Chakraborty, *Appl. Catal. A*, **505**, 548 (2015).

94. Z.-W. Wu, X. Li, Y.-H. Qin, L. Deng, C.-W. Wang and X. Jiang, *Int. J. Hydrogen Energy*, **45**, 15263 (2020).

95. P. Xie, Y. Yao, Z. Huang, Z. Liu, J. Zhang, T. Li, G. Wang, R. Shahbazian-Yassar, L. Hu and C. Wang, *Nat. Commun.*, **10**, 4011 (2019).

96. H. Muroyama, C. Saburi, T. Matsui and K. Eguchi, *Appl. Catal. A*, **443-444**, 119 (2012).

97. Z.-P. Hu, C.-C. Weng, C. Chen and Z.-Y. Yuan, *Appl. Catal. A*, **562**, 49 (2018).

98. H. Liu, H. Wang, J. Shen, Y. Sun and Z. Liu, *Appl. Catal. A*, **337**, 138 (2008).

99. D. V. Leybo, A. N. Baiguzhina, D. S. Muratov, D. I. Arkhipov, E. A. Kolesnikov, V. V. Levina, N. I. Kosova and D. V. Kuznetsov, *Int. J. Hydrogen Energy*, **41**, 3854 (2016).

100. I. Nakamura and T. Fujitani, *Appl. Catal. A*, **524**, 45 (2016).

101. H. Liu, H. Wang, J. Shen, Y. Sun and Z. Liu, *Catal. Today*, **131**, 444 (2008).

102. K. Okura, T. Okanishi, H. Muroyama, T. Matsui and K. Eguchi, *ChemCatChem*, **8**, 2988 (2016).

103. Q.-F. Deng, H. Zhang, X.-X. Hou, T.-Z. Ren and Z.-Y. Yuan, *Int. J. Hydrogen Energy*, **37**, 15901 (2012).

104. Z.-P. Hu, C.-C. Weng, G.-G. Yuan, X.-W. Lv and Z.-Y. Yuan, *Int. J. Hydrogen Energy*, **43**, 9663 (2018).

105. Q. Su, L. Gu, Y. Yao, J. Zhao, W. Ji, W. Ding and C.-T. Au, *Appl. Catal. B*, **201**, 451 (2017).

106. J. Zhao, L. Deng, W. Zheng, S. Xu, Q. Yu and X. Qiu, *Int. J. Hydrogen Energy*, **45**, 12244 (2020).

107. H. Zhang, Y. A. Alhamed, Y. Kojima, A. A. Al-Zahrani, H. Miyaoka and L. A. Petrov, *Int. J. Hydrogen Energy*, **39**, 277 (2014).

108. T. Meng, Q.-Q. Xu, Y.-T. Li, J.-L. Chang, T.-Z. Ren and Z.-Y. Yuan, *J. Ind. Eng. Chem.*, **32**, 373 (2015).

109. Y. Im, H. Muroyama, T. Matsui and K. Eguchi, *Int. J. Hydrogen Energy*, **45**, 26979 (2020).

110. J. Zhang, H. Xu, X. Jin, Q. Ge and W. Li, *Appl. Catal. A*, **290**, 87 (2005).

111. Y. Lu, H. Wang, Y. Liu, Q. Xue, L. Chen and M. He, *Lap Chip*, **7**, 133 (2007).

112. Y. Yi, L. Wang, Y. Guo, S. Sun and H. Guo, *AIChE J.*, **65**, 691 (2019).

113. C. Huang, H. Li, J. Yang, C. Wang, F. Hu, X. Wang, Z.-H. Lu, G. Feng and R. Zhang, *Appl. Surf. Sci.*, **478**, 708 (2019).

114. A. Srifa, K. Okura, T. Okanishi, H. Muroyama, T. Matsui and K. Eguchi, *Catal. Sci. Technol.*, **6**, 7495 (2016).

115. D. J. Haynes, D. Shekhawat, D. Berry, A. Roy and J. J. Spivey, *J. Rare Earths*, **38**, 711 (2020).

116. J.-L. Cao, Z.-L. Yan, Q.-F. Deng, Y. Wang, Z.-Y. Yuan, G. Sun, T.-K. Jia, X.-D. Wang, H. Bala and Z.-Y. Zhang, *Int. J. Hydrogen Energy*, **39**, 5747 (2014).

117. Y.-J. Lee, Y.-S. Lee, J. Y. Cha, Y. S. Jo, H. Jeong, H. Sohn, C. W. Yoon, Y. Kim, K.-B. Kim and S. W. Nam, *Int. J. Hydrogen Energy*, **45**, 19181 (2020).

118. I. Lucentini, I. Serrano, L. Soler, N. J. Divins and J. Llorca, *Appl. Catal. A*, **591**, 117382 (2020).

119. K. McCullough, T. Williams, K. Mingle, P. Jamshidi and J. Lauterbach, *Phys. Chem. Chem. Phys.*, **22**, 11174 (2020).

120. J. Cha, Y. S. Jo, H. Jeong, J. Han, S. W. Nam, K. H. Song and C. W. Yoon, *Appl. Energy*, **224**, 194 (2018).

121. G. Li, M. Kanezashi and T. Tsuru, *Catalysts*, **7**, 23 (2017)

122. X. Han, W. Chu, P. Ni, S.-z. Luo and T. Zhang, *J. Fuel Chem. Technol.*, **35**, 691 (2007).

Dr. Ho-Jeong Chae obtained B.S. degree in Chemical Engineering from Kyung Hee University, Korea, in 1995. He received M.S. and Ph.D degree in Chemical Engineering from Pohang University of Science and Technology (POSTECH), Korea, in 1997 and 2001, respectively. From 2001 to 2006, he was a senior researcher at Samsung Fine Chemical. He moved to LG Chem in 2006 and joined Korea Research Institute of Chemical Technology (KRICT) in 2007. He is currently a principal researcher in the Chemical & Process Technology Division of KRICT. He has published more than 60 papers and 80 international and domestic patents. He has been recognized with several awards including KRICT Star Award (2015), KRICT Innovation Award (2015), Green Star Award (2013), KRICT Excellent Employee Award (2012), Excellent Researcher Award (2007).